Z. Phys. C – Particles and Fields 35, 181–199 (1987)

Zeitschrift für Physik C Particles and Fields

Searches for Supersymmetric Particles with the CELLO Detector at PETRA

CELLO Collaboration

H.-J. Behrend, J. Bürger, L. Criegee, J.B. Dainton [1], H. Fenner, J.H. Field, G. Franke, J. Meyer, V. Schröder, U. Timm, G.G. Winter, W. Zimmermann
Deutsches Elektronen-Synchrotron, DESY, D-2000 Hamburg, Federal Republic of Germany

P.J. Bussey, C. Buttar, A.J. Campbell, D. Hendry, G. McCurrach, J.M. Scarr, I.O. Skillicorn, K.M. Smith
University of Glasgow, Glasgow G128QQ, UK

J. Ahme, V. Blobel, M. Feindt, J. Harjes, J.H. Peters, M. Poppe [2], H. Spitzer
II. Institut für Experimentalphysik, Universität Hamburg, D-2000 Hamburg, Federal Republic of Germany

W.-D. Apel, A. Böhrer, J. Engler, G. Flügge [3], D.C. Fries, J. Fuster [4], K. Gamerdinger, P. Grosse-Wiesmann [5], J. Hansmeyer, G. Hopp, H. Jung, J. Knapp, M. Krüger, H. Küster, P. Mayer, H. Müller, K.H. Ranitzsch, H. Schneider, J. Wolf
Kernforschungszentrum und Universität Karlsruhe, D-7500 Karlsruhe, Federal Republic of Germany

W. de Boer, G. Buschhorn, G. Grindhammer, B. Gunderson, Ch. Kiesling [6], R. Kotthaus, H. Kroha, D. Lüers, H. Oberlack, P. Schacht, G. Shooshtari, W. Wiedenmann
Max-Planck-Institut für Physik und Astrophysik, München, D-8000 München, Federal Republic of Germany

M. Davier, J.-F. Grivaz, J. Haissinski, P. Janot, V. Journé, F. Le Diberder, E. Ros [7], A. Spadafora [8], J.-J. Veillet
Laboratoire de l'Accélérateur Linéaire, F-91405 Orsay, France

R. George, N. Goldberg, O. Hamon, F. Kapusta, F. Kovacs, L. Poggiolo, M. Rivoal
Laboratoire de Physique Nucléaire et Hautes Energies, Université de Paris, F-75230 Paris, France

G. d'Agostini, F. Ferrarotto, M. Gaspero, B. Stella
University of Rome and INFN, I-00100 Rome, Italy

G. Cozzika, Y. Ducros, Y. Lavagne, F. Ould Saada [9], J. Žáček [10]
Centre d'Études Nucléaires, Saclay, F-91191 Gif-sur-Yvette, France

G. Alexander, G. Bella, Y. Gnat, J. Grunhaus, A. Klatchko, A. Levy
Tel Aviv University, Tel Aviv, Israel

Received 20 February 1987

[1] Permanent address: University of Liverpool, UK
[2] Now at CERN, Geneva, Switzerland
[3] Now at RWTH, Aachen, FRG
[4] Now at Universidad de Valencia, Spain
[5] Now at Stanford Linear Accelerator Center, Stanford, USA
[6] Heisenberg-Stipendiat der Deutschen Forschungsgemeinschaft
[7] Now at Universidad Autónoma de Madrid, Spain
[8] Now at Lawrence Berkeley Laboratory, Berkeley, USA
[9] Now at University of Hamburg, FRG
[10] Permanent address: Nuclear Center, Charles University, Prague, CSSR

Abstract. Mass limits are presented for various supersymmetric particles: scalar partners of electrons, muons, taus and quarks; photinos, winos and zinos. They were obtained from the analysis of an exposure of 48.6 pb^{-1} of the CELLO detector at the PETRA e^+e^- storage ring up to a center of mass energy of 46.8 GeV. Special attention has been given to the case where the photino is assumed to be the lightest supersymmetric particle, but other possibilities have also been considered.

Table 1. Minimal particle content of a supersymmetric theory

Spin	0	1/2	1	3/2	2
Matter multiplets	$\tilde{l}_L, \tilde{l}_R$	l			
	$\tilde{q}_L, \tilde{q}_R$	q			
		$\tilde{g}$	g		
		$\tilde{\gamma}$	γ		
Gauge multiplets	$h_w^{\pm}$	$\tilde{w}_1^{\pm}, \tilde{w}_2^{\pm}$	$W^{\pm}$		
	h_z^0	$\tilde{z}_1^0, \tilde{z}_2^0$	Z^0		
	h^0, A^0	$\tilde{h}^0$			
				$\tilde{G}$	G

1 Introduction

1.1 Theoretical Framework

The Standard Model of electroweak and strong interactions, based on the $SU(3)\otimes SU(2)\otimes U(1)$ gauge group with spontaneous $SU(2)\otimes U(1)$ breaking, has been confirmed by a vast amount of experimental data. However, for a number of reasons both aesthetic and theoretical, it is commonly accepted that this model cannot be the ultimate theory of elementary particles and of their interactions. This has led to various attempts at extension schemes among which one of the most promising seems to be supersymmetry. In particular, supersymmetric theories have improved convergence properties which may help to stabilize the low scale of electroweak symmetry breaking in the presence of other large scales in the theory (this is the so-called "hierarchy problem" inherent in Grand Unified Theories). Also, they shed a new light on the nature of the still mysterious Higgs sector and, in their local form, they provide a natural connection with gravitation.

One of the most striking features of supersymmetric models [1] is the prediction of multiplets of particles containing both bosons and fermions [2]. The minimal particle content of any supersymmetric model is displayed in Table 1. The equality of the numbers of bosonic and fermionic degrees of freedom within each supermultiplet is at the origin of the belief that supersymmetry may solve the gauge hierarchy problem [3]. More precisely, in the matter multiplets a scalar partner ($\tilde{q}_L, \tilde{q}_R, \tilde{l}_L, \tilde{l}_R$), often improperly called "left" or "right handed", is associated with each helicity state of the ordinary quarks or leptons. In the gauge multiplets, with each neutral massless gauge boson will be associated one Majorana gauge fermion, for instance the photino $\tilde{\gamma}$ with the photon, or a gluino $\tilde{g}$ with a gluon; with a neutral massive gauge boson, the Z^0, will be associated two Majorana gauge fermions, the zinos $\tilde{z}_1^0$ and $\tilde{z}_2^0$, and one Higgs scalar, the h_z^0; with a charged massive gauge boson, the $W^{\pm}$, will be associated two Dirac gauge fermions, the winos $\tilde{w}_1^{\pm}$ and $\tilde{w}_2^{\pm}$, and a charged Higgs scalar, the $h_w^{\pm}$. Supersymmetry therefore provides a framework for the unification between the gauge and Higgs sectors [4] within which zinos and winos are expected to have electroweak properties "half way" between those of gauge and Higgs bosons. In addition, since at least two Higgs doublets are needed within supersymmetry to give masses to both up and down-type quarks [5], resulting in three neutral and one charged physical states after the Z^0 and the $W^{\pm}$ have become massive, there still remain at least two neutral Higgs bosons, a scalar h^0 and an axion-like pseudoscalar A^0, which together are associated with a Majorana fermion, the higgsino $\tilde{h}^0$. Finally, when gravitation is taken into account, with the massless spin 2 graviton is associated a spin 3/2 gravitino $\tilde{G}$.

Supersymmetry, however, cannot be an exact symmetry in nature since we know, for instance, that there is no scalar particle degenerate in mass with the electron. Unfortunately, nothing is known a priori about the details of the symmetry breaking mechanism, and therefore about the mass splittings within the supermultiplets except that, if the hierarchy problem is actually to be solved, they cannot be very much in excess of the weak scale. If supersymmetry is realized globally, its spontaneous breaking will lead to a massless Goldstone fermion, the goldstino. If supersymmetry is realized locally in the framework of supergravity [6], the goldstino will be absorbed to give the $\pm 1/2$ polarization states of the gravitino when the latter acquires a mass as a result of the super-Higgs mechanism. Since the phenomenology of the goldstino is practically identical to that of a light gravitino [7], we will not consider the goldstino further in the rest of this article.

When supersymmetry is broken, not only are the supermultiplets split but mixing occurs between the electroweak eigenstates to form mass eigenstates [1]. Except perhaps for the supersymmetric partners of the top quark, it is usually expected that the amount of mixing is small between the "left" and "right-

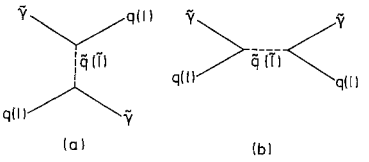

Fig. 1a, b. Feynman diagrams for the interaction of photinos with matter

handed" scalars, so that in practice they can be treated as mass eigenstates. This is an assumption that we will make throughout this article. As the mass differences between the "right" and "left-handed" scalars depend on the details of the supersymmetry breaking mechanism, we have considered in practice the two extreme possibilities, namely mass degeneracy ($M_R = M_L$) and very large splitting ($M_R \ll M_L$). As the two winos acquire different masses, the relative amounts of gaugino and higgsino components within them will be modified, and similarly for the two zinos. For convenience, we will simply call wino $\tilde{w}$ (zino $\tilde{z}$) the lighter of the two winos (zinos), even when it is more higgsino than gaugino-like. Furthermore, mixing may occur, but normally to a lesser extent, between photino, zinos, and higgsino [8]. This additional mixing will be neglected throughout this article, which means in particular that we will always consider that the physical photino is purely the supersymmetric partner of the photon. This hypothesis is found to be verified in a large class of broken supergravity models.

No freedom remains beyond that involved in the choice of a supersymmetry breaking mechanism. In particular, the couplings of the supersymmetric particles are completely determined by the field contents of the mass eigenstates.

For phenomenological studies, a very important feature present in most supersymmetric models is the absolute conservation of a multiplicative quantum number, R-parity [9]. Since $R = (-1)^{2S+3B-L}$, all ordinary particles have $R = 1$, whereas their supersymmetric partners have $R = -1$. As a consequence of R-parity conservation supersymmetric particles (SP's) are always produced in pairs and the decay of an SP always leads to an odd number of SP's, of which the lightest supersymmetric particle (LSP) is absolutely stable. In this article, we will always assume R-parity conservation.

Cosmological arguments lead to the conjecture that the LSP should be neutral and colorless [10], in which case the LSP can be the gravitino, the photino, the zino, the higgsino, or a scalar neutrino. Unless otherwise specified, we will assume that the LSP is one of these. The interaction of the LSP with ordinary matter then always turns out to be weak. For instance, if the LSP is a photino, this results from the fact that its interaction with a quark (lepton) is mediated by the exchange of a high mass scalar quark (lepton) [11], as depicted in Fig. 1. This is the reason for the universal line of search for supersymmetry: missing energy and momentum.

1.2 The Experiment

In this article, we report on extensive searches for supersymmetric particles performed using data collected with the CELLO detector at the e^+e^- storage ring PETRA operating at center of mass energies of up to 46.8 Gev. This is the highest value to date at which e^+e^- collisions have been analysed.

A detailed description of the CELLO detector can be found in [12]. Here, we recall only the main features, emphasizing those particularly relevant for supersymmetric particle searches.

As we have seen, the distinctive signature of supersymmetry is the missing energy and momentum carried away by the LSP's. CELLO features hermetic calorimetry down to a polar angle of 50 mrad with respect to the beam axis. For this purpose, the main component is a 20 radiation length thick lead liquid argon calorimeter, with fine lateral and longitudinal segmentation and sixfold sampling in depth. The 16 modules of the barrel part, located in a single cryostat, cover the polar angle domain $|\cos(\theta)| < 0.86$ while the 4 end cap modules span the range $0.92 < |\cos(\theta)| < 0.99$. The energy resolution for electromagnetic showers can be parametrized as $\delta E/E = 5\% + 10\%/\sqrt{E}$ (GeV).

The acceptance gap $0.86 < |\cos(\theta)| < 0.92$ between the barrel and end cap regions of the calorimeter was covered in the spring of 1984 with a lead scintillator sandwich, called the "hole tagger", segmented eightfold in azimuth, with two samplings after 4 and 8 radiation lengths. Although its energy resolution is rather poor, it can efficiently be used for vetoing purposes. Finally, at small angles, a lead glass array extends the electromagnetic calorimetry from 120 mrad, at the end of the end cap acceptance, down to 50 mrad.

The barrel calorimeter is located outside a thin superconducing solenoidal coil which provides a 1.3 T magnetic field, allowing charged particle momentum measurment by a set of interleaved drift and proportional chambers. The precision achieved with interaction vertex constraint is $\delta P_t/P_t = 1\%\ P_t$ (GeV/c) for $|\cos(\theta)| < 0.91$.

Electrons are identified by an energy deposition in the calorimeter compatible with their momentum measurement, and with a pattern characteristic of an electromagnetic shower. Muons are minimum ionizing in the calorimeter and, if above 1.4 GeV/c, they

Table 2. Data samples used in this analysis. Energies are in GeV, integrated luminosities in pb^{-1}

$\sqrt{\langle s \rangle}$	$\sqrt{s}$	$\int L dt$	Remarks
41.2	40.09–43.18	4.2	no hole tagger
44.2	43.15–45.22	3.4	
46.0	45.19–46.78	3.4	
44.2	44.2	9.2	hole tagger installed
46.6	46.6	1.1	
43.6	43.6	17.0	
43.45	43.45	1.4	
38.28	38.28	8.9	
43.0		$\sum$ 48.6	

penetrate the 80 cm thick iron absorber surrounding the detector and are detected in large planar drift chambers covering 92% of the solid angle.

A summary of the data samples used in the analyses presented in this article can be found in Table 2.

The main elements entering the trigger logic are:

- charged particle tracks in the central detector identified by a fast pattern recognition system,
- the energy depositions in each of the calorimeter modules, and
- a hit pattern from the barrel muon chambers.

The combinations relevant for the SP searches reported here were:

- one charged particle track and at least 2 GeV energy deposition in one barrel calorimeter module or
- an energy deposition of at least 2 GeV in each of two barrel modules separated by at least 45° in azimuth or
- an energy deposition of at least 3 GeV in one of the barrel modules or
- two charged particle tracks separated by at least 20° in azimuth and of which at least one is spatially correlated with a hit muon chamber. This trigger has been in operation only since the summer of 1985, in particular for the 17 pb^{-1} accumulated at 43.6 GeV.

The calorimeter trigger efficiencies were determined using electrons from radiative Bhabha scattering events independently triggered by a tag in the small angle or end cap calorimeters. The charged particle track trigger efficiency was measured using large angle Bhabha scattering events independently triggered in the calorimeter. The muon trigger efficiency was determined using the muon pair sample, as obtained from an independent trigger on collinear charged tracks.

2 Overall Strategy for Supersymmetric Particle Searches

Given a limited center of mass energy, the natural SP to search for in the first place is the LSP. However, if it is neutral as commonly expected, its pair production will lead to an undetectable final state, unless the technique of initial state radiation tagging is used, as first suggested for neutrino counting [13]. A detailed account of this search has already been published [14]. Since a charged SP usually has to be exchanged in such a reaction, as shown for example in Fig. 2e, the limits obtained this way on the LSP mass depend on the mass of the exchanged SP. There-

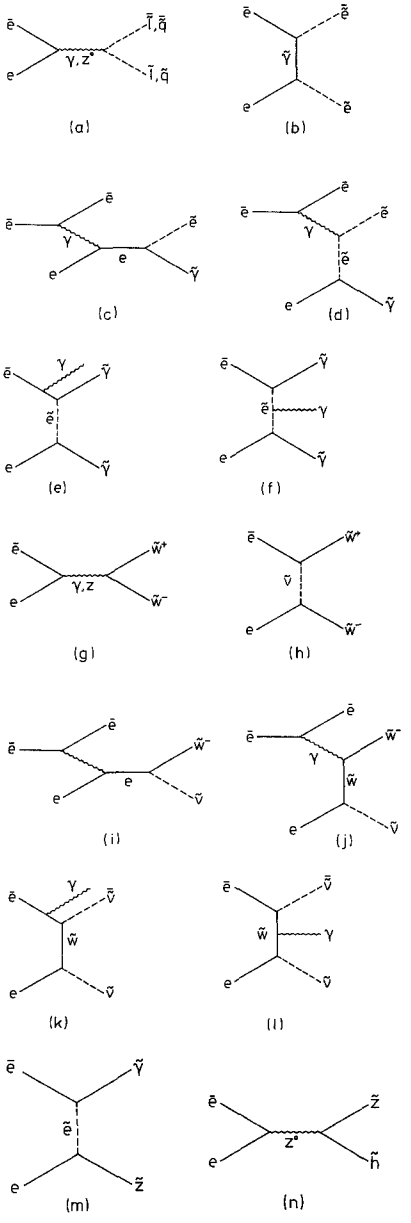

Fig. 2a–n. Diagrams for the production of supersymmetric particles in e^+e^- collisions

fore one may present the same results rather as limits on the masses of the exchanged particles, and this is the choice made in this article.

Unless otherwise specified, we make the usual assumption that the photino is the LSP, but will devote at the end a specific section to the discussion of the consequences of other choices. In addition, unless explicitly otherwise stated, we will assume that all decays cascading to the LSP are prompt, which is actually true if the photino is the LSP and if no particular phase space restriction occurs [15].

The search is then naturally directed toward the next-to-lightest supersymmetric particle (NLSP). If charged, it can be easily pair produced via one photon annihilation (see Figs. 2a and 2g). At PETRA energies, the corresponding production mechanism with Z^0 exchange can still be neglected in comparison. If the NLSP is either a gluino or a scalar neutrino, it will be very difficult to detect and, in such a case, the search will rather be directed toward the NNLSP (the next-to-next-to-lightest supersymmetric particle!). In practice, the exact hierarchy between photino and scalar neutrino as LSP and NLSP does not really matter since the decay will be invisible [16] in both cases ($\tilde{\nu} \to \nu\tilde{\gamma}$ or $\tilde{\gamma} \to \bar{\nu}\tilde{\nu}$).

We first investigate the production of charged matter scalars. Scalar electrons can be produced in pairs (see Figs. 2a, b), or singly in association with a photino (see Figs. 2c, d), or can affect the rate of radiative production of pairs of photinos (see Figs. 2e, f). All these cases are considered in Sect. 3. In contrast, scalar muons and taus can be produced at an observable rate only in pairs (see Fig. 2a). Their search is described in Sect. 4. Finally, scalar quark production (see Fig. 2a) is investigated in Sect. 5. Here the possibility that the gluino mass may be intermediate between the photino and the scalar quark masses plays a role in the analysis.

Having shown that the matter scalars are out of reach, we next turn to the search for the supersymmetric partners of the weak gauge bosons. These might well be lighter than their ordinary partners, as suggested by some supergravity inspired models [17]. Winos can be produced in pairs (see Figs. 2g, h), or singly in association with a scalar neutrino (see Figs. 2i, j), or can affect the rate of radiative scalar neutrino pair production (see Figs. 2k, l). Of course, the two latter cases are of interest only if the NLSP is a scalar neutrino. These wino searches are presented in Sect. 6. The threshold for zino production might be lower than that of wino pair production since zinos can be produced in association with photinos (see Fig. 2m). This is investigated in Sect. 7. In both the wino and the zino searches, the influence of the relative amounts of gaugino and higgsino within them is taken into account, and the possibility of a gluino mass intermediate between those of the photino and the wino or zino is considered.

Having failed to detect supersymmetric particles under the assumption that the photino is the LSP, we drop this hypothesis and consider the other possibilities in Sect. 8. If the LSP were a charged particle, it could be pair produced (see Figs. 2a and 2g), with a final state consisting of a pair of stable charged particles. This is investigated for completeness in 8.1 but, as mentioned in 1.1, it is unlikely that the LSP be charged. With a neutral LSP other than the photino, the possibility arises that the photino be the NLSP; since it would then decay, its production might be detected. The search for such unstable photinos is presented in 8.2. Given this unsuccessful search, it remains to investigate how the conclusions previously drawn in Sects. 3 to 7 under the hypothesis that the photino is the LSP are affected if the photino is neither the LSP nor the NLSP. This discussion is done in 8.3. If the LSP is the higgsino, a new reaction can take place: associated zino-higgsino production via s-channel Z^0 exchange (see Fig. 2n), the analysis of which is described in 8.4.

This completes our searches for supersymmetric particles, the results of which are summarized and compared with others in Sect. 9.

Typical SP production cross sections [18] are displayed in Fig. 3 in the case where the photino is the LSP. One can see that pair production of charged particles is copious, but with a mass limited to the beam energy; that associated production may give access to higher masses, but with smaller cross sections; and that this is even more the case for radiative production.

The following considerations apply to all the analyses discussed in this article:

- As already stated, the distinctive signature for supersymmetry is missing energy and momentum; however, since initial state radiation and gamma-gamma interactions tend to produce final states with missing momentum along the beam direction because of particles escaping undetected in the beam pipe, we made use of the missing transverse momentum, with respect to the beam axis, in order to enhance any signal of supersymmetry.

- The efficiency of each search was determined using a Monte-Carlo simulation of the reaction under investigation. Initial state radiation has been taken into account [19], which is particularly important for the pair production of particles with thresholds close to the beam energy. The Lund string fragmentation scheme [20] was used to model the hadronization of quarks and gluons. The response of the detector

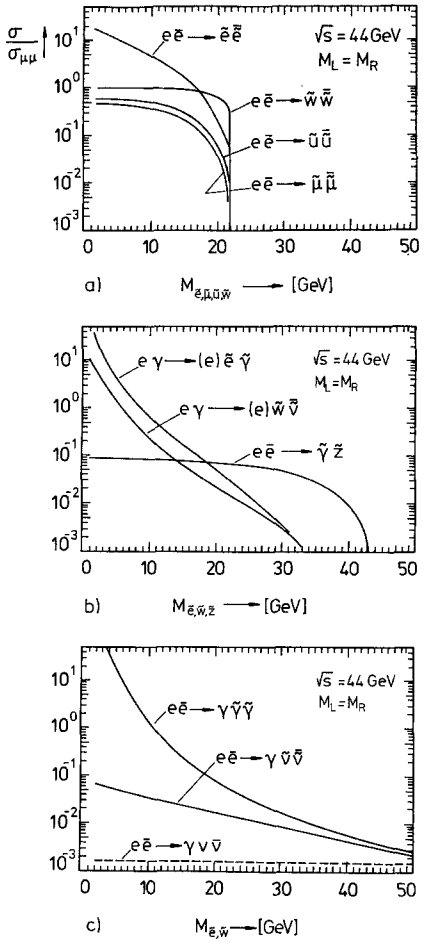

Fig. 3a–c. Supersymmetric particle production cross sections, relative to the μ pair cross section, for a beam energy of 22 GeV: **a** Pair production of scalar electrons and muons ($\tilde{e}$, $\tilde{\mu}$), scalar quarks with charge 2/3 ($\tilde{u}$), and winos ($\tilde{w}$). **b** Associated production. **c** Radiative production, with a photon acceptance as in our previous publication [14]. For comparison, the dashed line indicates the level of radiative production of neutrino pairs, for three flavours of neutrino. Photinos and scalar neutrinos are assumed massless where relevant. For $\tilde{\gamma}\tilde{z}$ production, $M_{\tilde{e}_R} = M_{\tilde{e}_L} = 50$ GeV is assumed

and of the reconstruction algorithms, the trigger requirements and the selection cuts were simulated in detail.

- All limits are given at the 95% confidence level.

3 Search for Scalar Electrons

3.1 Introduction

It is assumed in this section that the LSP is the photino and that the scalar electron decays promptly into an electron and a photino.

If the mass of a scalar electron is below the beam energy, it can be pair produced (see Figs. 2a, b) [21], the final state consisting of acoplanar electron pairs with missing energy and momentum carried away by the photinos. This search is described in Sect. 3.2.

Scalar electrons can also be produced singly in association with a photino and an electron (see Figs. 2c, d) [22]. In contrast to pair production, this process is sensitive to scalar electron masses above the beam energy. Here the dominant configuration is that where one of the beam electrons radiates a quasi real photon which interacts with an electron of the opposite beam, the radiating electron being scattered at very small angle and remaining undetected in the beam pipe. The decay of the scalar electron gives rise to an energetic electron which, for high scalar electron masses, is distributed fairly isotropically, and to an undetected photino. The observable final state will therefore consist of a single electron. This search is described in Sect. 3.3.

Finally, scalar electrons of even higher mass could be detected by their effect on the rate of the radiative production of photino pairs (see Figs. 2e, f) [23], where the detectable final state only consists of a single photon. We refer to our previous publication [14] for a report on this search.

3.2 Search for Acoplanar Electron Pairs

The following criteria were applied to select acoplanar electron pairs:

C1. Two tracks in the inner detector within $|\cos(\theta)| < 0.85$, and originating from the interaction vertex.

C2. Either the track momentum or the associated shower energy above 2.5 GeV for both tracks, or above 6 GeV for one track and above 1 GeV for the other.

C3. Acoplanarity of the two tracks between 35° and 170°. The acoplanarity is $180° - \phi$, where ϕ is the angle between the momenta of the two particles projected on the plane transverse to the beam direction. If the visible transverse momentum is conserved, the acoplanarity is 0.

C4. A missing transverse momentum above 3 GeV/c.

C5. No other shower visible in the barrel or end cap calorimeter.

C6. No hit in the hole tagger, or, for the data sample taken before the installation of the hole tagger, the missing momentum vector not pointing to the $|\cos(\theta)|$ range between 0.85 and 0.93.

Cut C3 removes Bhabha scattering and cuts C2, C3, and C4 efficiently remove electron pairs from $\gamma\gamma$ collisions. Radiative Bhabha scattering events are removed by the veto against additional photons (cuts C5 and C6).

No event was found satisfying these cuts.

3.3 Search for Single Electrons

The following criteria were applied to select single electron events:

C1. One track within $|\cos(\theta)| < 0.85$.

C2. An associated shower with transverse energy $E_t > 0.3 E_{\text{beam}}$.

C3. No other track, and no other shower in the barrel or in the end cap calorimeters.

C4. No signal in a hole tagger octant opposite to the track in azimuth.

C5. The track must not point in the transverse projection to the boundary between two calorimeter modules within ± 15 mrad.

Background from radiative Bhabha scattering with only one electron visible in the detector is removed efficiently by cut C2 which forces either the other electron or the photon into the end cap acceptance in order to balance the transverse momentum. Another potentially dangerous background comes from the "virtual Compton" configuration $e^+e^- \to e\gamma(e)$ where the spectator electron remains in the beam pipe and the photon goes into the gap between the barrel and the end cap calorimeters. This QED process can be removed either by kinematic reconstruction of the photon direction from the electron direction and energy, assuming that the second electron is scattered at zero degree, or by using the hole tagger as a veto against additional photons (cut C4). Without the hole tagger veto we would expect ~ 700 events with this kinematic configuration. For this reason, in this analysis we use only the data sample taken after the installation of the hole tagger. Cut C5 removes 3 "virtual Compton" events where the photon escapes through one of the 2 cm wide gaps between the barrel calorimeter modules.

After these cuts there is no candidate event left containing a single energetic electron.

3.4 Results

Using the cross section for the pair production of scalar electrons as given in [24] for arbitrary photino masses, the null result of the search for acoplanar electrons translates into the excluded domains limited by the contours labelled A in Figs. 4a and 4b, for $M_{\tilde{e}_R} \ll M_{\tilde{e}_L}$ and $M_{\tilde{e}_R} = M_{\tilde{e}_L}$, respectively.

To turn the result of the search for single electrons into limits on SP masses, we took the cross section for $\gamma e \to \tilde{\gamma}\tilde{e}$, as computed in [25] for arbitrary photino masses, and used the equivalent photon approximation [26]. The scalar electron and photino mass domains excluded by this analysis are limited by the contours labelled B in Fig. 4.

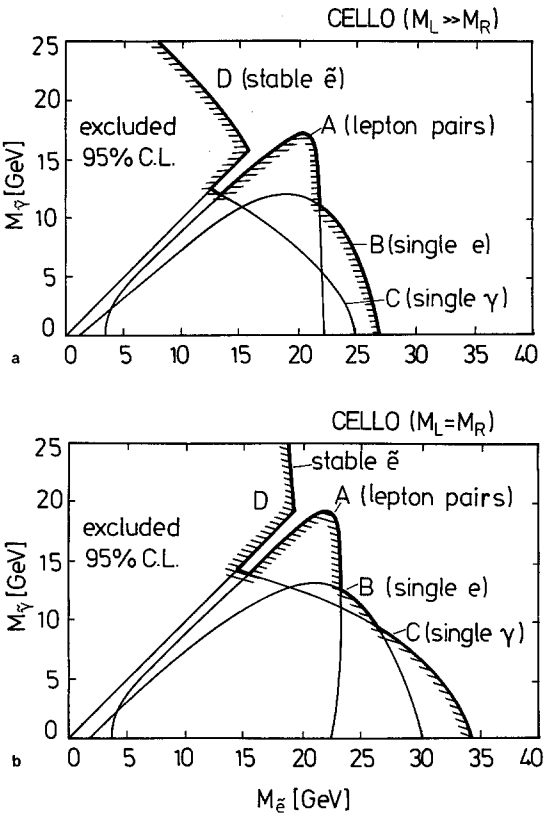

Fig. 4a, b. Scalar electron and photino mass domains excluded at the 95% CL for **a** $M_{\tilde{e}_L} \gg M_{\tilde{e}_R}$, **b** $M_{\tilde{e}_L} = M_{\tilde{e}_R}$. Contours A, B, C, limit the domains excluded by $\tilde{e}$ pair production, by $\tilde{e}\tilde{\gamma}$ associated production, and by radiative $\tilde{\gamma}$ pair production. Contour D limits the domain excluded for a stable $\tilde{e}$

The domains excluded by our search for single photons are limited by the contours labelled C in Fig. 4.

Altogether, we exclude $M_{\tilde{e}_R} = M_{\tilde{e}_L} < 34.2$ GeV *and* $M_{\tilde{e}_R} < 26.8$ GeV $\ll M_{\tilde{e}_L}$ *for massless photinos, and* $M_{\tilde{e}_R} = M_{\tilde{e}_L} < 26.1$ GeV *and* $M_{\tilde{e}_R} < 23.2$ GeV $\ll M_{\tilde{e}_L}$ *for* $M_{\tilde{\gamma}} = 10$ GeV.

8 Search for Scalar Muons and Scalar Taus

4.1 Introduction

It is assumed in this section that the LSP is the photino and that the scalar muon or tau decays promptly into its ordinary partner and a photino.

Scalar muons or taus can be pair produced as shown in Fig. 2a, leading to a final state consisting of a pair of acoplanar muons or taus with missing energy and momentum carried away by the photinos.

4.2 Search for Acoplanar Muon Pairs

The following criteria were applied to select acoplanar muon pairs from 17 pb^{-1} collected at 43.6 GeV after the installation of the muon trigger:

C1. Two tracks in the inner detector within $|\cos(\theta)|<0.85$, and originating from the interaction vertex.

C2. Momentum above 3 GeV/c and associated shower energy less than 1.3 GeV for both tracks.

C3. At least one track identified as a muon in the muon chambers.

C4. Acoplanarity of the two tracks between 20 and 160°.

C5. A missing transverse momentum of more than 4 GeV/c.

C6. No other shower visible in the barrel or end cap calorimeter, and no hit in the hole tagger.

Cuts C2, C4, and C5 reject the background from the two photon process $e^+e^-\to(ee)\mu\mu$. Radiative muon pair production $e^+e^-\to\mu\mu\gamma$ is vetoed by cut C6.

4.3. *Search for Acoplanar Tau Pairs*

We have searched for acoplanar taus in the two prong topology which covers 75% of tau pair decays [27]. The cuts are similar to those used in 3.2 for the selection of acoplanar electrons:

C1. Two tracks in the inner detector within $|\cos(\theta)|<0.85$, and originating from the interaction vertex.

C2. A momentum above 2.5 GeV for both tracks, or above 6 GeV for one track and above 1 GeV for the other.

C3. Acoplanarity of the two tracks between 35° and 170°.

C4. A missing transverse momentum, calculated from the two charged particles only, larger than 3 GeV/c.

C5. No additional photon in the barrel or end cap calorimeter, except if its invariant mass with any of the charged particles was smaller than 2 GeV, nor in the hole tagger.

C6. Acoplanarity of the jet axes, obtained by using both the tracks and the neutral particles, greater than 20°.

Cuts C2, C3, and C4 reject the background from the two photon process $e^+e^-\to(ee)\tau\tau$. Radiative lepton pair production $e^+e^-\to\tau\tau\gamma$, $\mu\mu\gamma$ and $ee\gamma$ is vetoed by cut C5. In order to reject these events efficiently, we used only the data sample taken after the installation of the hole tagger. Cut C6 removes events from tau pair production with two very acoplanar tracks of which one has a low momentum.

After these cuts, no candidate event remains.

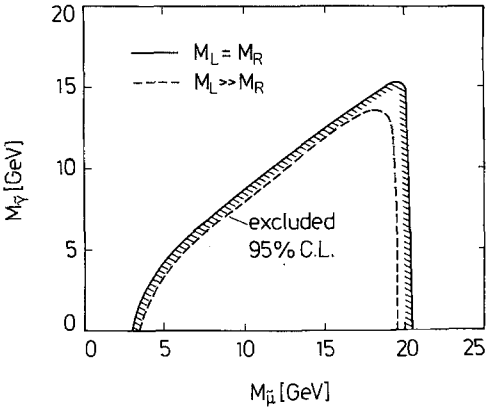

Fig. 5. Scalar muon and photino mass domains excluded at the 95% CL for $M_{\tilde{\mu}_L}=M_{\tilde{\mu}_R}$ (full curve) and $M_{\tilde{\mu}_L}\gg M_{\tilde{\mu}_R}$ (dashed curve)

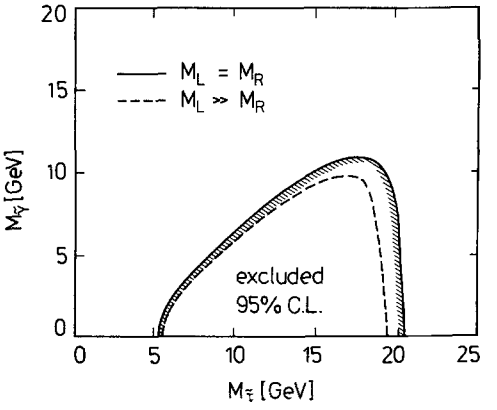

Fig. 6. Scalar tau and photino mass domains excluded at the 95% CL for $M_{\tilde{\tau}_L}=M_{\tilde{\tau}_R}$ (full curve) and $M_{\tilde{\tau}_L}\gg M_{\tilde{\gamma}_R}$ (dashed curve)

4.4 *Results*

The results of our searches for acoplanar muons(taus), with an efficiency of $\sim 20\%$ ($\sim 10\%$) for masses around 20 GeV, translate into excluded mass domains as shown in Fig. 5 (Fig. 6).

In particular, for scalar muons $2.8<M_{\tilde{\mu}_R}=M_{\tilde{\mu}_L}<20.5$ GeV *and* $3.4<M_{\tilde{\mu}_R}<19.4$ GeV $\ll M_{\tilde{\mu}_L}$ *are excluded for* $M_{\tilde{\gamma}}=0$. *Similarly, for scalar taus* $5.3<M_{\tilde{\tau}_R}=M_{\tilde{\tau}_L}<20.6$ GeV *and* $5.6<M_{\tilde{\tau}_R}<19.5$ GeV $\ll M_{\tilde{\tau}_L}$ *are excluded.*

5 Search for Scalar Quarks

5.1 *Introduction*

In this Section, we assume that the LSP is the photino, and investigate the pair production of scalar quarks (see Fig. 2a). The scalar quark will normally decay to a quark and a photino, in which case the final state will consist of hadron jets with missing energy and momentum. However, if the gluino is the NLSP, the scalar quark will rather decay to a quark and a gluino, because the $\tilde{q}q\tilde{g}$ strong coupling is large compared to the $\tilde{q}q\tilde{\gamma}$ electromagnetic coupling. With the subsequent decay $\tilde{g}\to q\bar{q}\tilde{\gamma}$, the final state will then

consist of 6 "jets" with relatively little missing energy, leading to rather spherical multihadronic events.

5.2 Search for Jets with Missing Energy and Momentum

The following requirements have been made:

C1. At least 5 charged particle tracks within $|\cos(\theta)|<0.85$, originating from the interaction point and with a transverse momentum $p_t>120$ MeV/c.

C2. A total visible energy (from charged and neutral particles) larger than $0.15\sqrt{s}$, and an energy deposited in the barrel calorimeter larger than $0.07\sqrt{s}$.

C3. A total missing energy larger than $0.45\sqrt{s}$, and a transverse missing momentum larger than $0.18\sqrt{s}$.

C4. A missing momentum vector and a sphericity axis both within $|\cos(\theta)|<0.80$.

C5. The opening angle between the transverse missing momentum vector and the transverse momentum of any particle (charged or neutral) $>30°$.

Cuts C3 and C5 efficiently reduce the background from tau pair production, from $\gamma\gamma$ interactions and inelastic Compton scattering, and from e^+e^- annihilation into multihadrons. Events produced with a hard radiated photon are removed by cut C4. All the events satisfying the above cuts were scanned and those obviously from an interaction of a beam particle with the residual gas or with the beam pipe were removed. One "monojet" like event, shown in Fig. 7, remains, with all tracks concentrated in a narrow cone. It may be interpreted as resulting from quark pair production with hard initial state radiation, the photon escaping through one of the 2 cm wide gaps between the barrel calorimeter lead modules. In our data sample we expect ~ 0.6 event of this type. This event was kept as a candidate for limit calculations.

5.3 Search for an Excess of Spherical Events

The CELLO standard multihadronic event selection procedure is described in [28]. We choose to characterize spherical events by their large aplanarity $A = 3 \times E_1/2$, where E_1 is the smallest eigenvalue of the sphericity tensor. For $\sqrt{s}$ above 34 GeV the fraction of events with $A>0.1$ was found to be rather constant ($\sim 4\%$).

5.4 Results and Discussion

We present results for the two decay scenarios discussed in Sect. 5.1, distinguishing whether the gluino is heavier or lighter than the scalar quark. Only one flavour of charge 2/3 scalar quarks was assumed to be produced. We have considered the case of mass degenerate "left" and "right handed" scalar quarks, and that of a lighter "right handed" scalar quark only. The latter possibility is expected in some supergravity models [29] where the lightest scalar quark is actually the "right handed" scalar top, possibly lighter than its ordinary partner. In this case, the direct decay to $t\tilde{\gamma}(\tilde{g})$ is kinematically forbidden and the dominant decay mode is expected to be to $c\tilde{\gamma}(\tilde{g})$ [30].

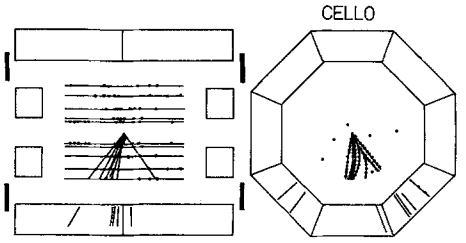

Fig. 7. The "monojet" candidate event. Its most likely origin is radiative quark pair production, with the photon escaping through a gap between two of the calorimeter modules

5.4.1 Heavy Gluino. In this case the topology to investigate is that of jets with missing energy and momentum. For light photinos, the detection efficiency decreases from 35% for a scalar quark mass of 20 GeV to 2% for a mass of 8 GeV. For larger photino masses, the efficiency decreases because of the lower visible energy. We have systematically assumed that the scalar quark electromagnetic decay occurs before its hadronization. However, this assumption is of little consequence since the R-hadron formed during the fragmentation process would anyway keep most of the initial scalar quark momentum, which implies that the missing momentum carried away by the photino would be essentially unaffected.

We exclude the following domains: for $M_{\tilde{\gamma}}=0$, $2.1 < M_{\tilde{q}_R}=M_{\tilde{q}_L}<21.5$ GeV and $2.2<M_{\tilde{q}_R}<21.2$ GeV $\ll M_{\tilde{q}_L}$ *on the one hand; and, for* $M_{\tilde{\gamma}}=10$ GeV, $12.5 < M_{\tilde{q}_R}=M_{\tilde{q}_L}<21.3$ GeV *and* $13.3<M_{\tilde{q}_R}<20.8$ GeV $\ll M_{\tilde{q}_L}$ *on the other.*

5.4.2 Light Gluino. In this case the relevant search is for spherical events. The detection efficiency for events resulting from scalar quark pair production turns out to be similar to the one of normal multihadronic events for masses around 20 GeV. This is because the gain in acceptance due to the $\sin^2(\theta)$ angular distribution of spin 0 particle pair production, as compared to the $1+\cos^2(\theta)$ distribution for normal spin 1/2 quarks, is compensated by a radiative correction factor which is smaller when the center of mass energy is not too far above the scalar quark threshold.

The variable used in this search, namely the aplanarity, simply measures the average momentum out

of the event plane. The aplanarity is therefore rather insensitive to the fraction of 3-jet events. On the other hand, it does depend on the fraction of n-jet events ($n>3$) and, as our Monte-Carlo program generates jets only up to the second order of QCD, we have no reliable estimate for the contribution to the aplanarity from higher order QCD processes.

Thus, we have used the following strategy:

- light scalar quarks could be detected as an excess in the total hadronic cross section; this will allow us to exclude any scalar quark production up to a certain center of mass energy;
- we then use the data at that energy to obtain an estimate of the higher order QCD contribution, and conservatively use this estimate at higher center of mass energies;
- this will then allow us to set an upper limit to any abnormal contribution to the sample of aplanar events.

From a fit to the combined results from various PEP and PETRA experiments [28] on the total hadronic cross section in the center of mass range between 14 and 46.8 GeV, a single "right handed" scalar quark was excluded up to 13.7 GeV, assuming, to be conservative, a small value for α_s ($\Lambda_{\mathrm{QCD}}=10$ MeV) so that most of the excess over the quark parton model prediction be attributed to scalar quark production. Knowing then that no scalar quark threshold could have occured below 27 GeV, we proceeded to search for a threshold effect at a higher energy by fitting simultaneously the strong coupling constant α_s and the scalar quark mass, fixing $\sin^2\theta_W$ at its world average value of 0.23. Scalar quark masses up to 15.5 GeV could be excluded this way. The correlation between α_s and the scalar quark mass was found to be weak (0.1), as expected since the QCD contribution decreases with increasing energy while the scalar quark contribution would increase. If two mass degenerate scalar quarks contribute, the limit becomes 18.5 GeV. Knowing that a light scalar quark with a mass below ~ 15 GeV is excluded, we used the CELLO high energy data to perform in an analogous way a fit to the cross section for events with an aplanarity larger than 0.1, as a function of the center of mass energy.

The scalar quark mass lower limit then improves to 20.3 GeV *if* $M_{\tilde{q}_L}=M_{\tilde{q}_R}$, *and to* 19.2 GeV *if* $M_{\tilde{q}_L} \gg M_{\tilde{q}_R}$.

6 Search for Winos

6.1 Introduction

Winos can be pair produced by one photon exchange (see Fig. 2g) irrespective of their gaugino-higgsino content. The contribution from t-channel scalar neutrino exchange (see Fig. 2h) which depends on the scalar neutrino mass and, because of the small electron mass, only involves the gaugino component of the wino at the $e\tilde{\nu}\tilde{w}$ vertices, always increases the cross section [31]. Neglecting it can therefore only yield safer limits.

In associated wino-scalar neutrino production (see Figs. 2i, j), only the gaugino component of the wino contributes. This is also the case for the radiative production of pairs of scalar neutrinos by wino exchange (see Fig. 2k, l).

6.2 Wino Decay Scenarios and Search Strategy

The decay of the wino will depend both on its gaugino-higgsino content and on the detailed SP mass hierarchy. We assume in this section that the photino is the LSP. Three scenarios are then to be considered.

6.2.1 Heavy Gluino, Heavy Scalar Neutrino. If the wino is the NLSP, it will decay to a photino and a virtual W (see Figs. 8a and 8b) or to a neutrino and a virtual scalar lepton (see Fig. 8c) or to a quark and a virtual scalar quark (see Fig. 8d). In all cases, this will result in a lepton or a $q\bar{q}$ pair with missing momentum. Within this scenario, searches for acoplanar pair of leptons (possibly not of the same flavour) or jets are relevant to investigate wino pair production.

6.2.2 Light Gluino. If the gluino is the NLSP and the wino the NNLSP, the dominant decay mechanism will be to $q\bar{q}\tilde{g}$ (see Fig. 8e), unless the exchanged scalar quark is substantially heavier than the W. This is because the $\tilde{q}q\tilde{g}$ strong coupling is large compared to the $\tilde{q}q\tilde{\gamma}$ electromagnetic coupling. With the subsequent decay $\tilde{g}\to q\bar{q}\tilde{\gamma}$, the result will be 4 "jets" for each wino, with small missing momentum. A search for spherical multihadronic events is relevant in this case to investigate wino pair production.

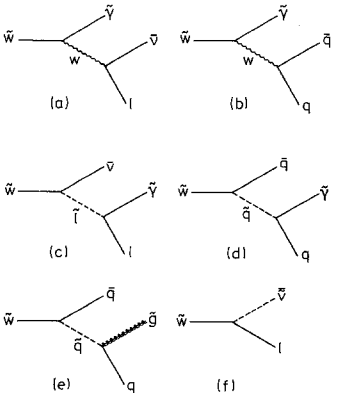

Fig. 8a–f. Diagrams for wino decays

6.2.3 Light Scalar Neutrino. If the scalar neutrino is the NLSP and the wino the NNLSP, the wino will exclusively decay to a scalar neutrino and its associated lepton (see Fig. 8f). As the scalar neutrino decays invisibly to $\tilde{\gamma}\nu$, the final state will consist of a lepton with missing momentum, and, if the wino has a large higgsino component this lepton will preferentially be a tau. Searches for acoplanar lepton pairs are also relevant in this case to investigate wino pair production.

For light enough scalar neutrinos, and if the gaugino content of the wino is substantial, associated wino-scalar neutrino production may give access to wino masses higher than the beam energy, in contrast to wino pair production. As already explained in 3.1 for associated photino-scalar electron production, this is accompanied by an undetected spectator electron and will therefore lead to a single lepton in the final state. With the CELLO trigger conditions given in Sect. 1.2, a search for single electrons is practical in this case.

The radiative production of pairs of scalar neutrinos via wino exchange may give access to still higher wino masses, again only if the gaugino content in the wino is substantial. Here the final state will consist of a single photon, and we refer to our previous publication for this analysis [14].

6.3 Event Selections

We first list the Sections in which event selections relevant to the wino searches have already been described:

- Acoplanar electron pairs in 3.2.
- Acoplanar muon pairs in 4.2.
- Acoplanar tau pairs in 4.3.
- Spherical events in 5.3.
- Single electrons in 3.3.

The search for acoplanar electron pairs is actually also sensitive to acoplanar $e\mu$ pairs.

The search for jets with missing energy and momentum described in Sect. 5.2 is well adapted to a two body decay ($\tilde{q} \to q\tilde{\gamma}$), but it would lead to a lower efficiency in the present case of a three body decay ($\tilde{w} \to q\bar{q}\tilde{\gamma}$) because of the smaller missing energy. Instead, the following specific search has been performed, with more emphasis on the jet acoplanarity than on the missing energy. The following requirements were first made:

C1. A total energy of a least 2 GeV in the barrel liquid argon calorimeter.

C2. At least one track within $|\cos(\theta)| < 0.85$ originating from the interaction point and with a transverse momentum $p_t > 400$ MeV/c, and one additional track with $p_t > 120$ MeV/c, and a total energy of the charged particle tracks above $0.05\sqrt{s}$.

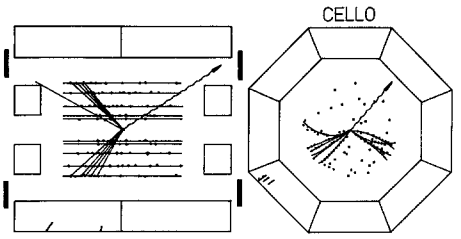

Fig. 9. An acoplanar jet event, rejected as a candidate for supersymmetric particle production, because of an additional hard photon in the hole tagger (wiggled line), suggesting radiative quark pair production

All particle momenta were then projected onto the plane perpendicular to the beam axis ($R-\phi$ projection). The event was divided into two half planes in the $R-\phi$ projection by a line passing through the interaction point and normal to the thrust axis of the projected momenta.

The following cuts were then applied:

C3. At least two charged particles in each half plane.

C4. A total visible energy from charged and neutral particles larger than $0.30\sqrt{s}$.

C5. An acoplanarity above 50°, of the vectorial sums of the transverse momenta of the particles belonging to each half plane.

C6. No hard photon in the hole tagger. (Fig. 9 shows such an acoplanar jet event rejected because of an additional hard photon hitting the hole tagger.)

Residual background events from beam gas interactions were removed by scanning. After the scan, we are left with one candidate event, recorded before the installation of the hole tagger. A Monte Carlo study shows that in our data sample we expect ~ 1.2 such events from normal quark pair production. We kept this event as a candidate for limit calculations.

6.4 Results and Discussion

In this Section, we follow the scheme outlined in Sect. 6.2.

6.4.1 Heavy Gluino, Heavy Scalar Neutrino. In this case, only pair production is relevant, and in order to get results valid irrespective of the gaugino-higgsino content within the wino we considered only the contribution from one photon annihilation.

To interpret the result of our searches for acoplanar lepton pairs, we took into account both W exchange (see Fig. 8a) and scalar lepton exchange (see Fig. 8c) in the wino decay. In the latter case we assumed a scalar lepton mass of 100 GeV, and modified

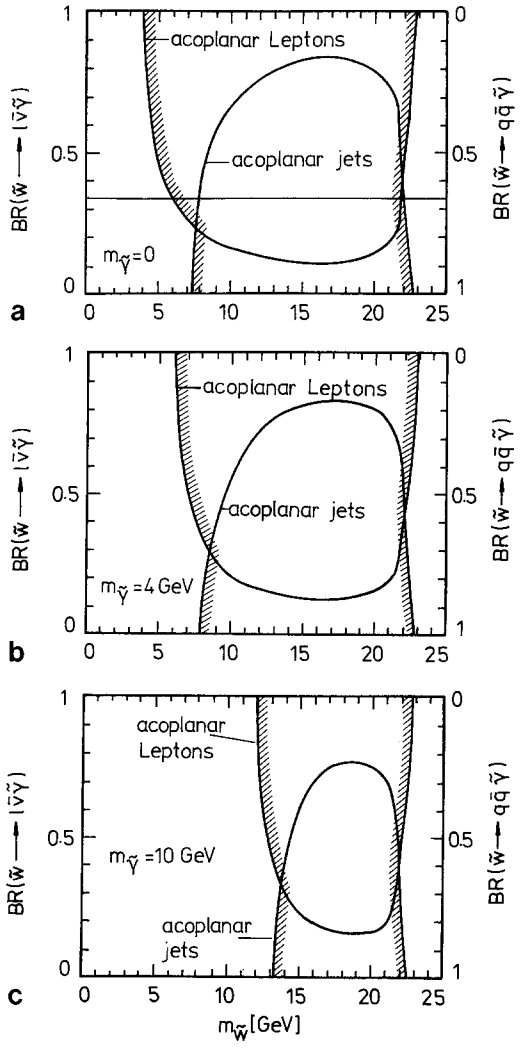

Fig. 10a–c. Wino masses excluded at the 95% CL, as a function of the leptonic branching ratio, for the case where both $\tilde{g}$ and $\tilde{\nu}$ are heavy: **a** $M_{\tilde{\gamma}}=0$ GeV, **b** $M_{\tilde{\gamma}}=4$ GeV, **c** $M_{\tilde{\gamma}}=10$ GeV. The horizontal line in **a** indicates a leptonic branching ratio of $3\times 11\%$ as expected for a wino decaying via W exchange

the $\tilde{z}$ decay matrix element given in [36]. For small photino masses the detection efficiency for acoplanar ee and $e\mu$ events from $\tilde{w}$ decays rises continuously from $\sim 2.5\%$ for $M_{\tilde{w}}=4$ GeV to $\sim 45\%$ for $M_{\tilde{w}}=21$ GeV and turns out to be independent of the wino decaying via W or scalar lepton exchange. The efficiency decreases for photino masses close to the wino mass because the decay leptons in this case have little energy. Figure 10 shows the wino masses excluded as a function of the leptonic branching ratio assuming equal decay widths into e, μ, and τ, for $M_{\tilde{\gamma}}=0$, 4, and 10 GeV. If the wino decay proceeds dominantly via W exchange, a branching ratio of $3\times 11\%$ into leptons is expected (horizontal line in Fig. 10a). If the decay via scalar quark or lepton exchange is dominant one expects BR$(\tilde{w}\to l\bar{\nu}\tilde{\gamma})\sim 3\times 16\%$ for the case of equal scalar quark and lepton masses.

The result of the acoplanar jet search is interpreted similarly in terms of the mechanisms shown in Figs. 8b–d. The detection efficiency rises from 1.6% at $M_{\tilde{w}}=10$ GeV to 13% for $M_{\tilde{w}}=21$ GeV ($M_{\tilde{\gamma}}=4$ GeV). Again, the detection efficiency is insensitive to the wino decaying via W or via scalar quark exchange. Wino mass domains excluded by these searches are also shown in Fig. 10.

It can be seen in Fig. 10a that, from the combined search for leptonic and hadronic final states, $7.5<M_{\tilde{w}}<22.4$ GeV *can be excluded for massless photinos*, independently of the leptonic branching ratio. Because they are essentially restricted by phase space, no improvement of these limits is obtained by considering the cases where one of the winos decays leptonically and the other hadronically. The upper bound of the excluded domain shows little sensitivity to the photino mass.

6.4.2 Light Gluino. Here also, only pair production is relevant. For $\tilde{w}$ masses close to the beam energy, the efficiency of wino detection in our search for multihadronic events is $\sim 87\%$. From the total hadronic cross section one can exclude wino masses below 21 GeV in the same way as explained in the search for scalar quarks (Sect. 5.4.2). Similarly, the absence of an excess of spherical events at the highest PETRA energy (see Sect. 5.3), sets *a mass lower limit of* 22.4 GeV for winos decaying mostly to $q\bar{q}\tilde{g}$ (see Fig. 8e). This limit is not sensitive to the gluino mass and does not depend on the QCD background of spherical events, as explained in Sect. 5.4.2.

6.4.3 Light Scalar Neutrino. Here the only decay mechanism to consider is that shown in Fig. 8f.

Our searches for acoplanar lepton pairs, relevant for wino pair production, exclude the domain of wino and scalar neutrino masses limited by the contour labelled A in Fig. 11 for a wino predominantly gaugino-like, assuming equal decay widths into e, μ, and τ. If the wino is mostly higgsino-like, only acoplanar taus are to be taken into account and the contour limiting the excluded domain becomes that labelled H in Fig. 11.

To interpret the result of the search for single electrons, we used the cross section for $\gamma e\to\tilde{w}\tilde{\nu}$ given in [32] and the equivalent photon approximation [26]. A conservative estimate is obtained this way, since a full calculation taking into account all possible diagrams [33] systematically leads to a higher cross section. Our detection efficiency is around 70% for $\tilde{w}$ masses above the beam energy. For a wino purely gaugino and assuming an electronic branching ratio of 1/3, as expected if the three flavours of scalar neutrinos are mass degenerate, the domain limited by the contour labelled B in Fig. 11 could be excluded.

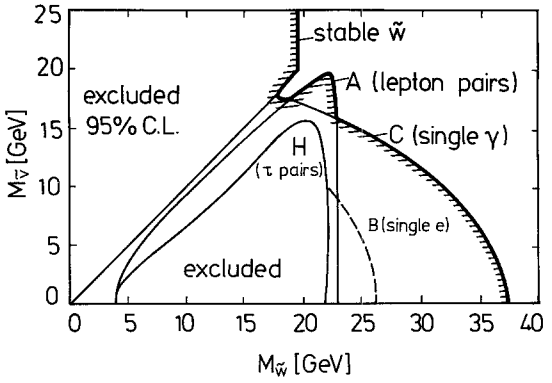

Fig. 11. Wino and scalar neutrino mass domains excluded at the 95% CL for the case of a light scalar neutrino. Contours A, B, C limit the domains excluded by $\tilde{w}$ pair production, by associated $\tilde{w}\tilde{\nu}$ production, and by radiative $\tilde{\nu}$ pair production, all in the case of a wino mostly gaugino-like, and with equal decay widths into e, μ and τ. Contour H limits the domain excluded by $\tilde{w}$ pair production, for a wino decaying exclusively to $\tau\tilde{\nu}$, as expected if it is mostly higgsino-like

Any higgsino admixture will reduce this domain.

A similar statement holds for the domain limited by the contour labelled C, excluded by our search for single photons [14] which is relevant for radiative scalar neutrino pair production by wino exchange.

Altogether, for massless scalar neutrinos, we exclude winos purely gaugino-like with $M_{\tilde{w}} < 37.3$ GeV, *and winos purely higgsino-like with* $3.9 < M_{\tilde{w}} < 21.5$ GeV.

7 Search for Zinos

7.1 Introduction

Zinos can be produced by t-channel exchange of scalar electrons in association with photinos (see Fig. 2m). Because of the small electron mass, only the gaugino component of the zino contributes to this reaction.

As in the case of the wino, the zino decay will depend both on its gaugino-higgsino content and on the detailed SP mass hierarchy. We assume in this section that the photino is the LSP. The zino may then decay to a pair of acoplanar leptons of the same flavour (see Fig. 12a) or of jets (see Fig. 12b). The two jets may even merge to form a "monojet" if the zino is sufficiently light. If the gluino is lighter than the zino, the dominant decay will be to $q\bar{q}\tilde{g}$ (see Fig. 12c) followed by $\tilde{g} \to q\bar{q}\tilde{\gamma}$, as already discussed in the case of the wino. Finally, if the scalar neutrino is lighter than the zino, the latter will decay exclusively to invisible final states (see Fig. 12d), and the initial state radiation tagging technique has again to be used [14].

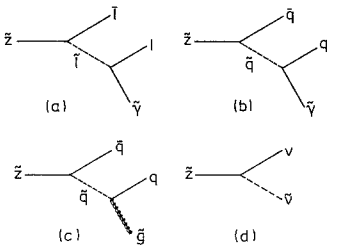

Fig. 12a–d. Diagrams for zino decays

Therefore, to investigate this reaction we can use the results of our searches for acoplanar electrons (Sect. 3.2) and for acoplanar jets (Sect. 6.3). In addition, a specific search for monojet topologies has been carried out to study this channel.

7.2 Search for Monojets

After performing the preselection defined by criteria C1 and C2 in Sect. 6.3 (search for acoplanar jets), single jets were selected by requiring:

C3. One half of the $R-\phi$ projection plane without charged particles and with at most 0.5 GeV in the electromagnetic calorimeter.

C4. A missing transverse momentum exceeding $0.15\sqrt{s}$.

C5. No hard photon in the hole tagger.

Multihadronic final states from $e^+e^- \to q\bar{q}(g)$ and from $\gamma\gamma$ collisions tend to be balanced in p_t and are efficiently removed by cut C4. More details can be found in our previous publication on monojet searches [34]. Residual background from beam gas interactions was removed by scanning. After the scan we are left with one candidate, already shown in Fig. 7. This event was kept as a candidate for limit calculations.

7.3 Results and Discussion

We assume here that the zino is a pure gaugino. Any higgsino admixture will lower the production cross-section and degrade the limits obtained accordingly. We also assume $M_{\tilde{e}_L} = M_{\tilde{e}_R}$; if $M_{\tilde{e}_L} \gg M_{\tilde{e}_R}$, the cross section should be reduced by a factor of ~ 2. We used the production cross-section as given in [35] and, for the zino decay, the matrix element given in [36].

7.3.1 Heavy Gluino, Heavy Scalar Neutrino. For scalar electron masses above the zino mass and for small photino masses, the detection efficiency for acoplanar electron pairs rises from $\sim 28\%$ at $M_{\tilde{z}} = 5$ GeV to $\sim 40\%$ for zino masses above 15 GeV. It varies only slowly with the scalar electron mass. For $M_{\tilde{e}} < M_{\tilde{z}}$ the zino can decay into an electron and a real scalar

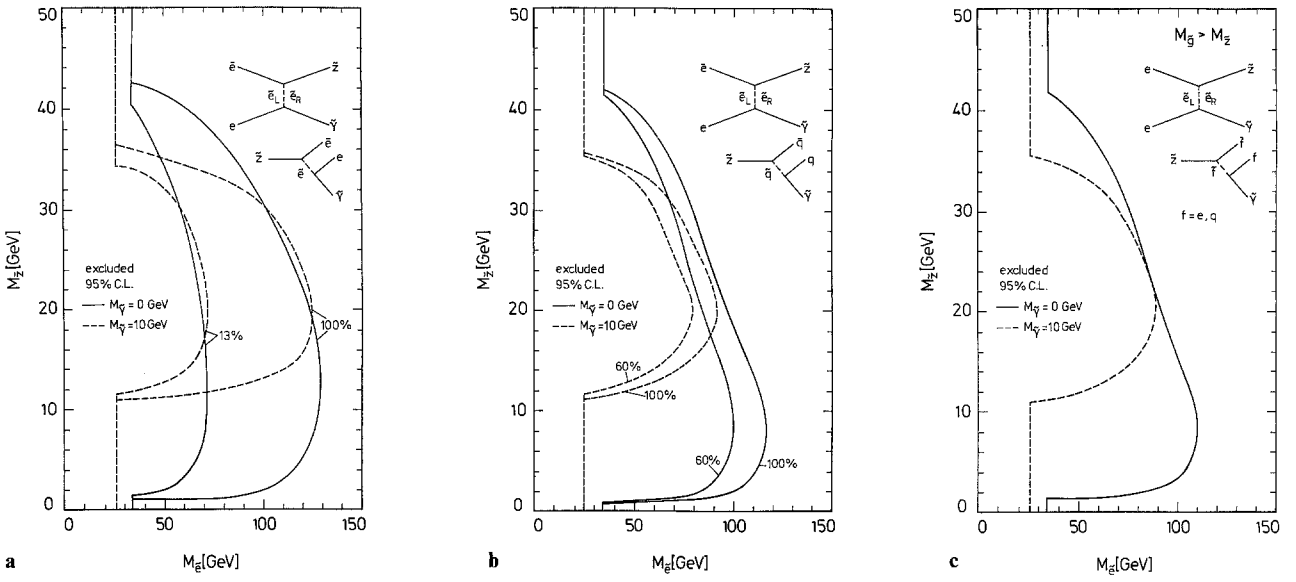

Fig. 13a–c. Zino and scalar electron mass domains excluded at the 95% CL, for a zino mostly gaugino-like, assuming $M_{\tilde{e}_L} = M_{\tilde{e}_R}$. Scalar electron masses below 34.2 GeV (26.1 GeV) are excluded for $M_{\tilde{\gamma}} = 0$ ($M_{\tilde{\gamma}} = 10$ GeV) by our $\tilde{e}$ search. **a** domain excluded if $\tilde{z} \to e e \tilde{\gamma}$ with $M_{\tilde{\gamma}} = 0$ (full lines) and $M_{\tilde{\gamma}} = 10$ GeV (dashed lines) for two different branching ratios: 100% and 13%. **b** domain excluded if $\tilde{z} \to q \bar{q} \tilde{\gamma}$ with $M_{\tilde{\gamma}} = 0$ (full lines) and $M_{\tilde{\gamma}} = 10$ GeV (dashed lines for two different branching ratios: 100% and 60%. **c** domain excluded from the combination of $\tilde{z} \to e e \tilde{\gamma}$ and $\tilde{z} \to q \bar{q} \tilde{\gamma}$ assuming a hadronic branching ratio of 60% with $M_{\tilde{\gamma}} = 0$ (full line) and $M_{\tilde{\gamma}} = 10$ GeV (dashed line)

electron. This leads to a variation of the detection efficiency for $M_{\tilde{e}} = M_{\tilde{z}}$. A scalar electron mass only slightly smaller than the zino mass leads to a soft electron from the zino decay together with an energetic electron from the decay of the scalar electron. Generally, the detection efficiency is $\sim 50\%$ if the scalar electron is lighter than the zino. As stated in Sect. 3.2, no acoplanar electron pair was found. Figure 13a shows the excluded zino and scalar electron mass domains assuming $M_{\tilde{\gamma}} = 0$ (full lines) and $M_{\tilde{\gamma}} = 10$ GeV (dashed lines). Scalar electron masses below 34.2 GeV (26.1 GeV) were already excluded for $M_{\tilde{\gamma}} = 0$ GeV (10 GeV) by our search for scalar electrons, as indicated by the vertical lines in Fig. 13a. Contours are shown for 100% and 13% zino branching ratios into electrons. If all scalar partners of quarks and leptons have equal masses, the expected branching ratios of the zino into quarks and leptons can be calculated from the known couplings. One then expects $\mathrm{BR}(\tilde{z} \to e e \tilde{\gamma}) \sim 13\%$ if $M_{\tilde{e}} > M_{\tilde{z}}$ and $\sim 3.5\%$ if $M_{\tilde{e}} < M_{\tilde{z}}$.

As far as the searches for hadronic final states are concerned, the efficiency of the monojet selection has a maximum of $\sim 45\%$ for $M_{\tilde{z}} \sim 10$ GeV and drops to $\sim 18\%$ for $M_{\tilde{z}} = 40$ GeV. The acoplanar jet selection efficiency rises from $\sim 3\%$ at $M_{\tilde{z}} = 15$ GeV to 13% at $M_{\tilde{z}} = 40$ GeV. The combined efficiency varies between 30% and 45% and is insensitive to the scalar electron and scalar quark masses. Zino masses excluded by this analysis are shown in Fig. 13b as a function of the scalar electron mass for branching ratios into $q \bar{q} \tilde{\gamma}$ of 100% and 60%, the latter being expected if all scalar quarks and leptons have equal masses. The full and dashed lines correspond to a massless and to a 10 GeV mass photino, respectively.

Figure 13c shows the combined limit for $\tilde{z} \to q \bar{q} \tilde{\gamma}$ and $\tilde{z} \to e e \tilde{\gamma}$, assuming a leptonic branching ratio of 13% per lepton generation. Since we consider both leptonic and hadronic final states this result is insensitive to variations in the leptonic branching ratio. *For* $M_{\tilde{e}_L} = M_{\tilde{e}_R} < 70$ GeV, *zino masses below* ~ 31 GeV *are excluded, with little dependence on* $M_{\tilde{\gamma}} < \sim 10$ GeV.

7.3.2 Light Gluino. In this case, the detection efficiency of the single jet selection drops rapidly from $\sim 50\%$ at low zino masses to below 4% for zino masses above 25 GeV while the acoplanar jet selection starts to become sensitive for zino masses above beam enery. The combined detection probability varies between 50% at low zino masses and $\sim 20\%$ for zino masses above the beam energy and is almost independent of the scalar quark and lepton masses. Figure 14 shows zino mass domains excluded by this analysis for gluino mass assignments of 5 and 10 GeV. In both cases we have taken $M_{\tilde{\gamma}} = 0$. The contours are shown for a 100% branching ratio into $q \bar{q} \tilde{g}$ since this decay, if kinematically possible, is expected to be dominant. *Again, for* $M_{\tilde{e}_L} = M_{\tilde{e}_R} < 70$ GeV, *zino masses below* ~ 30 GeV *are excluded.*

7.3.3 Light Scalar Neutrino. In this case, as the zino decays invisibly (see Fig. 12d), radiative zino pair production has to be used: our single photon search [14] excludes mass domains as shown in Fig. 15. For massless photinos, no domain in zino and scalar electron

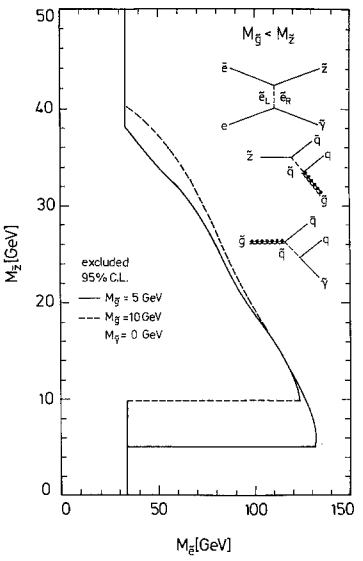

Fig. 14. Zino and scalar electron mass domains excluded at the 95% CL, for a zino mostly gaugino-like, if $\tilde{z} \to q\bar{q}\tilde{g}$ with $M_{\tilde{g}} = 5$ GeV (full line) and $M_{\tilde{g}} = 10$ GeV (dashed line) for a 100% branching ratio into $q\bar{q}\tilde{g}$. $M_{\tilde{e}_L} = M_{\tilde{e}_R}$ is assumed. Scalar electron masses below 34.2 GeV are excluded for $M_{\tilde{\gamma}} = 0$ by our $\tilde{e}$ search

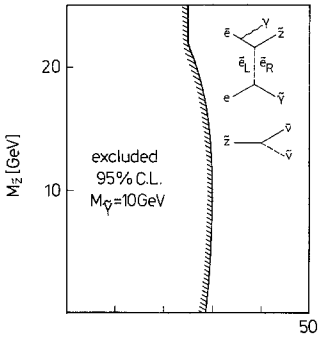

Fig. 15. Zino and scalar electron mass domains excluded at the 95% CL, for a zino mostly gaugino-like, if $\tilde{z} \to \nu\bar{\nu}$ for $M_{\tilde{\gamma}} = 10$ GeV. $M_{\tilde{e}_L} = M_{\tilde{e}_R}$ is assumed. Scalar electron masses below 26.1 GeV are excluded for $M_{\tilde{\gamma}} = 10$ GeV by our $\tilde{e}$ search

masses extends in the region not already excluded by the scalar electron search. *For* $M_{\tilde{\gamma}} = 10$ GeV, *zino masses below* ~ 22 GeV *are excluded for* $M_{\tilde{e}_L} = M_{\tilde{e}_R} = 26$ GeV, *but no excluded region remains for scalar electron masses above* 30 GeV.

8 What if the Photino is not the Lightest Supersymmetric Particle?

Having failed to detect any signal for supersymmetry under the assumption that the photino is the LSP, we are led to contemplate the other possibilities. We will consider in turn:

- a charged LSP.
- a neutral LSP, with the photino as NLSP.
- a neutral LSP, with a heavy photino.

8.1 Search for Charged Stable Supersymmetric Particles

In this section, we investigate the possibility that the LSP be a charged stable particle. As for any charged SP, the dominant production mechanism will be pair production via *s*-channel one photon exchange (see Fig. 2a and 2g). In addition, if the produced LSP is a scalar electron, *t*-channel photino exchange will also contribute (see Fig. 2b); and similarly scalar neutrino exchange for wino pair production (see Fig. 2h). However, in the latter case, because of the small electron mass, the *t*-channel exchange contribution is reduced by the a priori arbitrary amount of higgsino component within the wino. Since the interference between the diagrams shown in Figs. 2g and 2h is always constructive [31], we will ignore the contribution from scalar neutrino exchange to obtain safe limits on wino production, independent of its gaugino content.

Pair production of new charged stable particles will appear in CELLO as an excess in the muon pair production cross section. We have measured [37] $R_{\mu\mu} = \sigma_{\mu\mu}/\sigma_{\text{QED}} = 0.98 \pm 0.04 \pm 0.04$ at $\sqrt{s} = 43.0$ GeV, where $\sigma_{\text{QED}} = 4\pi\alpha^2/3s$. The momentum and acceptance cuts applied in this analysis were $p > 10$ GeV/c and $|\cos(\theta)| < 0.85$ for both tracks.

This result translates into a lower limit of 19.6 GeV *for the mass of a stable wino, and of* 15.4 GeV *or* 17.6 GeV *for a stable scalar muon (or tau), depending whether* $M_R \ll M_L$ *or* $M_R = M_L$. Using the production cross section given in [24], scalar electron and photino mass domains can be excluded, bounded by the contours labelled D in Figs. 4a and 4b for $M_{\tilde{e}_R} \ll M_{\tilde{e}_L}$ and $M_{\tilde{e}_R} = M_{\tilde{e}_L}$, respectively.

Although the possibility exists that a scalar quark, in particular a scalar top, be the LSP, we did not perform this analysis, the result of which would strongly depend on the scalar quark hadronization model.

8.2 Search for Unstable Photinos

In almost all the cases where the photino is considered unstable, its dominant decay is to a photon accompanied by an escaping LSP. Particularly noteworthy examples are $\tilde{\gamma} \to \tilde{G}\gamma$ [38] and $\tilde{\gamma} \to \tilde{h}^0\gamma$ [39]. There is an important exception if the LSP is a scalar neutrino but, as already indicated, the phenomenology would then be the same as for the opposite mass hierarchy. The case of a light zino is very similar to that of a light higgsino.

8.2.1 Promptly Decaying Photinos. We will first assume that the photino lifetime is sufficiently short for its flight path to be negligible.

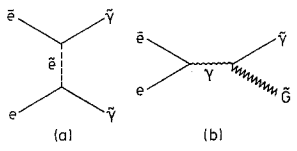

Fig. 16a, b. Diagrams for $\tilde{\gamma}$ pair production, and for $\tilde{\gamma}\tilde{G}$ associated production

Photinos can be pair produced via t-channel scalar electron exchange (see Fig. 16a). The final state is then two photons with missing energy. Depending on the photino mass, one expects two different types of event topologies. As their mass is increased, the photinos tend to decay more and more isotropically in the center of mass system, giving rise to two acoplanar photons; if the photinos are light, the decay products are boosted in the photino directions, which results in two nearly collinear photons, however with missing energy.

To select these topologies, the following selection criteria were applied to a 33.7 pb^{-1} data sample:

C1. No track in the inner detector.

C2. Two showers with an opening angle exceeding 15°.

C3. Each shower with an energy >2 GeV, within $|\cos(\theta)|<0.85$ and fiducial cuts at the calorimeter module edges.

C4. No hit in the hole tagger.

Cosmic showers have been suppressed by timing cuts on the calorimeter energy signals and by cuts on the shower direction and longitudinal development. A more detailed description of these cuts can be found in [14, 40]. The losses related to the cosmic rejection procedure were determined using as control sample the collinear photon pairs.

After the cosmic rejection, two classes of events were selected, one for heavy photinos (a) and one for light photinos (b):

- (a) acoplanarity between 10° and 165°
- (b) acoplanarity $<10°$ and acollinearity $<20°$ and the sum of the energies of the two photons $<1.5E_{\text{beam}}$.

No candidate event remains.

The region in photino and scalar electron masses excluded by this analysis is shown in Fig. 17a, for $M_{\tilde{e}_L}=M_{\tilde{e}_R}$ and using the cross section given in [41]. *For* $M_{\tilde{e}_L}=M_{\tilde{e}_R}=100$ GeV, *photino masses below* 15 GeV *are excluded.*

8.2.2 The Role of the Scale of Supersymmetry Breaking. We now take explicitly into account the finite lifetime of the produced photinos, restricting our analysis to the case where the LSP is the gravitino (if the LSP is the higgsino, the effects of finite lifetime become noticeable for photino masses lower than a few hundred MeV [39]).

The photino lifetime [38] and the gravitino mass [7] are related to the scale d of supersymmetry breaking: $\tau_{\tilde{\gamma}}=8\pi d^2/M_{\tilde{\gamma}}^5$ and $M_{\tilde{G}}=\sqrt{(8\pi G_N)}d/\sqrt{6}$, where

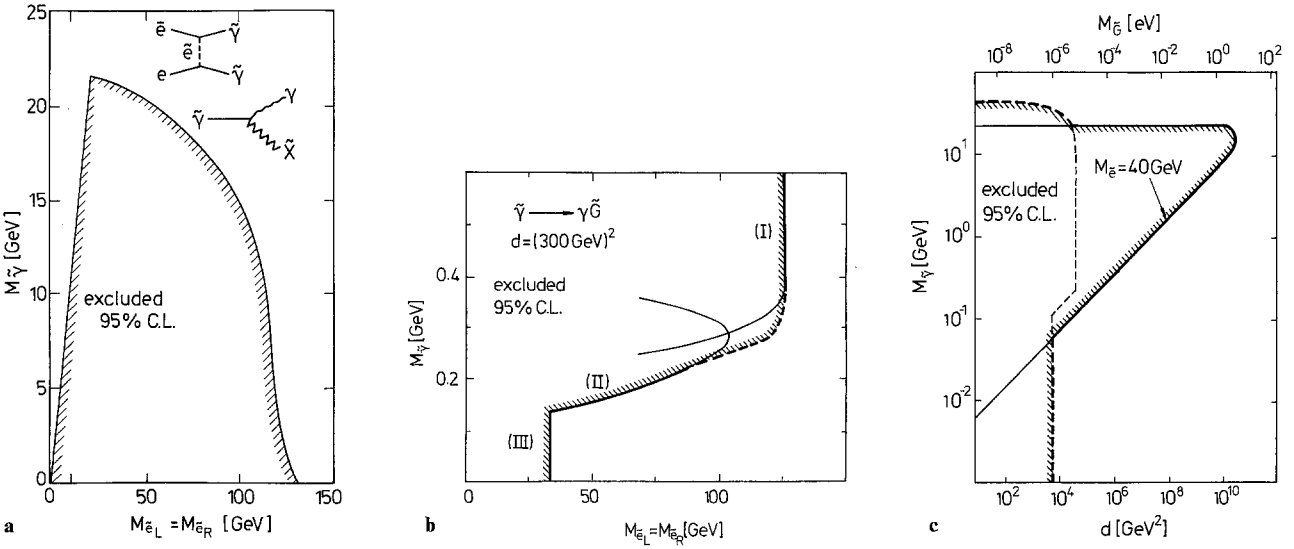

Fig. 17a–c. a Photino and scalar electron masses excluded at the 95% CL for promptly decaying photinos. **b** As in **a** for photinos decaying into a photon and a gravitino, but taking into account the finite lifetime, and assuming $d=(300\,\text{GeV})^2$: Contour I is the result obtained from pair production of photinos with both photinos decaying inside the detector. $M_{\tilde{e}_L}=M_{\tilde{e}_R}$ is assumed. Contour II is the same, but with only one photino decaying inside the detector. Contour III is the same, but with both photinos escaping the detector, thus using the radiated photon tagging technique. The dashed contour limits the domain excluded by the combination of these results. **c** Unstable photino masses excluded at the 95% CL as a function of the scale parameter d or of the gravitino mass $M_{\tilde{G}}$. The full line results from $\tilde{\gamma}$ pair production for $M_{\tilde{e}_L}=M_{\tilde{e}_R}=40$ GeV. The dashed contour results from the study of associated photino-gravitino production, and is independent of the scalar electron mass

G_N is the Newton constant. For $d=(300\ \text{GeV})^2$, that is $M_{\tilde{G}}=1.5\cdot10^{-5}$ eV, the photino must have a mass of at least 300 MeV to have a decay length $\gamma\beta c\tau<1$ m. Figure 17b (contour I) shows the modification to be brought to Fig. 17a when the finite photino lifetime is taken into account, and $d=(300\ \text{GeV})^2$.

This analysis can be improved toward smaller photino masses (i.e. longer lifetimes) by taking into account the topology where only one of the two photinos decays inside the detector. In this case, the visible final state will consist of a single photon. The results of our search for single photon events [14] exclude the domain limited by contour II in Fig. 17b.

For still longer lifetimes both photinos will escape the detector before decaying. However this case can still be analysed by using the initial state radiation tagging technique [23], and our single photon search can therefore be used to exclude the domain limited by contour III in Fig. 17b.

Up to now we have presented our results for a fixed value of $d=(300\ \text{GeV})^2$. We can equally well exclude a domain of photino masses as a function of the scale parameter d for a given value of the scalar electron mass. This is shown in Fig. 17c (full line) for $M_{\tilde{e}_R}=M_{\tilde{e}_L}=40$ GeV. The upper bound is due to phase space limitation, the lower bound to the requirement that at least one photino must decay within the detector. However, the excluded domain vanishes for $M_{\tilde{e}_L}=M_{\tilde{e}_R}>130$ GeV.

An interesting result can still be obtained even in this case by studying the associated production of a photino and a gravitino [23, 42], since this process can proceed via s-channel one photon exchange (see Fig. 16b, as obtained from $\tilde{\gamma}\to\tilde{G}\gamma$ by crossing). One has to distinguish again two cases: a short $\tilde{\gamma}$ lifetime leading to a single decay photon in the final state, and a long $\tilde{\gamma}$ lifetime necessitating the use of the initial state radiation tagging procedure. Using once more the result of our search for single photons, *we exclude* $d<(80\ \text{GeV})^2$ *for* $M_{\tilde{\gamma}}<35$ GeV, *and* $d<(225\ \text{GeV})^2$ *for* 200 MeV $<M_{\tilde{\gamma}}<10$ GeV. This result, which is independent of the scalar electron mass, is shown in Fig. 17c as a dashed line.

8.3 The Case of Heavy Photinos

We now suppose that the photino is too heavy to play a role in the search for supersymmetric particles at PETRA energies, and we will consider the other neutral colorless LSP candidates.

If the LSP is a scalar neutrino [43]:

- Scalar leptons will decay to their associated scalar neutrino and to a virtual W in a way very similar to the wino decays shown in Figs. 8a and 8b. The limits on scalar electrons, muons and taus therefore become similar to those obtained for the wino in Sect. 6.4.1, slightly worse however since scalars rather than fermions are pair produced here.
- No attempt was made to infer from the analyses described in Sect. 5 a scalar quark mass limit in the unlikely case that it is the NLSP. However, the limit derived if the gluino is the NLSP should be essentially unaffected.
- Naturally, the limits derived in Sects. 6.4.3 and 7.3.3 for the wino and the zino in the case of a light scalar neutrino are unaffected.

If the LSP is the gravitino, and if it is not vanishingly light, it practically decouples [7]. The NLSP then effectively plays the role of the LSP, and no additional discussion is therefore needed in this case.

If the LSP is a very light gravitino, or a zino, or a higgsino:

- The limits derived in Sects. 4 and 5 for scalar muons, taus and quarks are practically unaltered.
- The limits obtained in Sect. 3 from associated $\tilde{e}\tilde{\gamma}$ production and from photino pair production no longer apply. In addition, since in scalar electron pair production the t-channel photino exchange is now depressed by the higher photino mass, the mass limits on scalar electrons become similar to those obtained for scalar muons or taus, probably slightly better because of a higher detection efficiency.
- The limits obtained in Sect. 6 for the wino are practically unaffected.
- The limits obtained in Sect. 7 from the associated production of a photino and a zino no longer apply. However, if the LSP is the higgsino, a new production mechanism for zinos, in association with higgsinos, can take place; this is discussed in the next Section.

8.4 Associated Zino-Higgsino Production

It is assumed here that the LSP is the higgsino, in which case associated zino-higgsino production may be kinematically allowed, and occur via s-channel Z^0 exchange as shown in Fig. 2n. The Z^0 decay width into $\tilde{z}\tilde{h}^0$ is given in [44]. With subsequent $\tilde{z}\to ee\tilde{h}^0$ or $q\bar{q}\tilde{h}^0$ decays, proceeding via Z^0 exchange as shown in Fig. 18, the analysis in 7.3.1 applies with minor modifications. *A zino mass lower limit of* 31.3 GeV *is then set in the most favorable case where the zino*

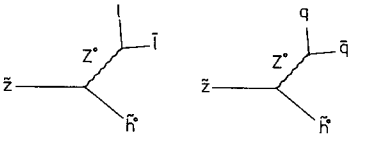

Fig. 18. Diagrams for $\tilde{z}$ decays, if the LSP is the higgsino

is purely higgsino-like, and assuming $M_{\tilde{h}^0}=0$. This limit is degraded by any gaugino admixture in the zino, or if the higgsino becomes massive.

9 Summary and Conslusions

In a broad search for supersymmetric particle production in e^+e^- reactions up to a center of mass energy of 46.8 GeV, no positive signal has been observed, and a comprehensive set of mass limits has been derived. The results presented in this article and in [14] supersede those reported in previous CELLO publications [45].

Given the unavoidable complexity involved in the presentation of supersymmetric particle (SP) mass limits if one wishes to take into account all possible choices for the lightest supersymmetric particle (LSP), we prefer to summarize and discuss our results under the single but also most common assumption that the LSP is the photino. Figure 19 shows the domains excluded, at the 95% CL, for the masses of various SPs. Our results are presented assuming a massless photino on the one hand (with a light gluino where relevant: $\tilde{q}$, $\tilde{w}$, $\tilde{z}$), and for a photino mass of 10 GeV (with a heavy gluino) on the other; the scalar neutrinos are assumed not to be significantly lighter than the charged scalar leptons.

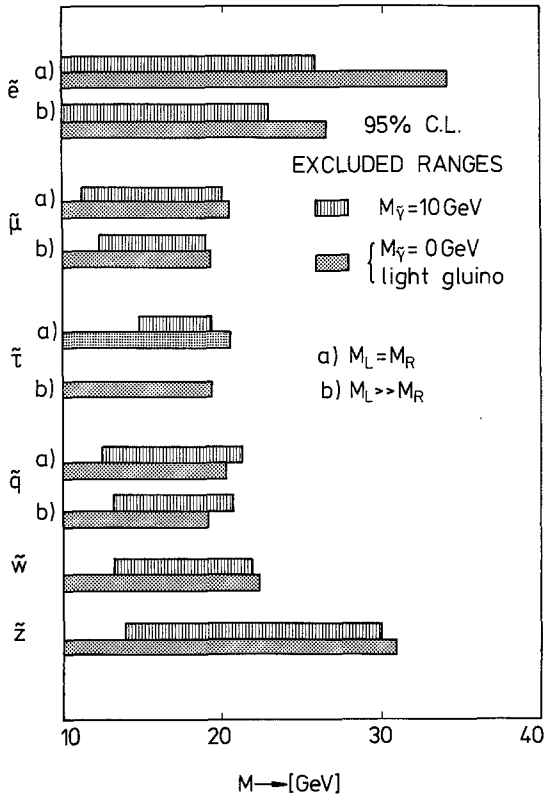

Fig. 19. Supersymmetric particle mass domains excluded at 95% CL by the analyses reported here, assuming that the photino is the LSP with two assumptions on the mass : $M_{\tilde{\gamma}}=10$ GeV (and a heavy $\tilde{g}$), and for massless photinos (with a light $\tilde{g}$). The wino mass limits have been computed, in the case of massless photinos, for a leptonic branching ratio of 1/3. The zino mass limits have been computed for $M_{\tilde{e}_L}=M_{\tilde{e}_R}=70$ GeV

Some of these limits ($\tilde{\mu}$, $\tilde{\tau}$, $\tilde{q}$, $\tilde{w}$) are fundamentally restricted by the available center of mass energy. As far as e^+e^- experiments are concerned, the best limits therefore come from PETRA (this article and [46, 47]), and they should not be improved in the near future, at least until sufficient data has been collected at TRISTAN or SLC. Some others are essentially limited by the accumulated luminosity, namely those which result from the search for a t-channel propagator effect ($\tilde{e}$ for massless photinos). In this case, the best present limits come from PEP [47, 48], but the CELLO results should be significantly improved with the analysis of the 1986 run at 35 GeV center of mass energy in which a luminosity of $\sim 90\ \mathrm{pb}^{-1}$ has been accumulated. Finally, some limits suffer from both limitations ($\tilde{e}$ for higher photino masses, $\tilde{z}$); in this case, the most constraining results come from PETRA.

As far as non e^+e^- experiments are concerned, the most stringent limits come from the UA1 experiment [49] at the CERN $p\bar{p}$ collider, but up to now results have been presented only for scalar quarks and gluinos. For the other supersymmetric particles, it is unlikely that mass limits at the level of those obtained in e^+e^- experiments will be obtained at hadron colliders in the short run, except perhaps for the wino from the search for the decay $W^{\pm}\to\tilde{w}\tilde{\gamma}$.

Although no evidence for supersymmetric particles has been found with the present machine energies and luminosities, supersymmetric theories still keep their attractive properties. Continuing the investigation will therefore remain worthwhile with the next generation of colliders.

Acknowledgements. We gratefully acknowledge the outstanding efforts of the PETRA machine group which made possible these measurements. We are indebted to the DESY computer centre for their excellent support during the experiment. We acknowledge the invaluable effort of many engineers and technicians from the collaborating institutions in the construction and maintenance of the apparatus, in particular the operation of the magnet system by M. Clausen, P. Röpnack, and the cryogenic group. We thank Dr. K.H. Pape for his assistance with our IBM emulator. The visiting groups wish to thank the DESY Directorate for the support and kind hospitality extended to them.

This work was partially supported by the Bundesministerium für Forschung und Technologie (Germany), the Commissariat à l'Energie Atomique and the Institut National de Physique Nucléaire et de Physique des Particules (France), the Istituto Nazionale di Fisica Nuclear (Italy), the Science and Engineering Research Council (UK), and the Israeli Ministry of Science and Development.

References

1. For introductions to the phenomenology of supersymmetry, see for instance: H.E. Haber, G. Kane: Phys. Rep. **117C**, 75 (1985); R.M. Barnett: Proc. of the 1985 SLAC Summer Institute on Particle Physics and extensive lists of references therein
2. P. Fayet: Unification of the Fundamental Particle Interactions, (Eds.) S. Ferrara, J. Ellis, P, Van Nieuwenhuizen. New York: Plenum Press 1980, p. 587
3. E. Witten: Nucl. Phys. **B188**, 513 (1981); S. Dimopoulos, H. Georgi: Nucl. Phys. **B193**, 150 (1981); N. Sakai: Z. Phys. C – Particles and Fields **11**, 153 (1981)
4. P. Fayet: Nucl. Phys. **B237**, 367 (1984)
5. K. Inoue et al.: Prog. Theor. Phys. **67**, 927 (1982), (E: **70**, 330 (1983), **71**, 413 (1984)), see also [3]
6. For a review, see: H.P. Nilles: Phys. Rep. **110C**, 1 (1984)
7. P. Fayet: Phys. Lett. **70B**, 461 (1977)
8. J. Ellis, G.G. Ross: Phys. Lett. **117B**, 397 (1982)
9. G. Farrar, P. Fayet: Phys. Lett. **76B**, 575 (1978), see also [2]
10. J. Ellis et al.: Nucl. Phys. **B238**, 453 (1984)
11. P. Fayet: Phys. Lett. **86B**, 272 (1979)
12. CELLO Coll., H.J. Behrend et al.: Phys. Scr. **23**, 610 (1981)
13. E. Ma, J. Okada: Phys. Rev. Lett. **41**, 287 (1978)
14. CELLO Coll., H.J. Behrend et al.: Phys. Lett. **176B**, 247 (1986)
15. I. Hinchliffe, L. Littenberg: Proc. of the DPF Summer Study on Elementary Particle Physics and Future Facilities. (Eds. R. Donaldson, F. Paige), p. 242. Fermilab: 1982
16. R.M. Barnett, H.E. Haber, K.S. Lackner: Phys. Lett. **126B**, 64 (1983), Phys. Rev. **D29**, 1990 (1984), see also [15]
17. S. Weinberg: Phys. Rev. Lett. **50**, 387 (1983); R. Arnowitt, A.H. Chamseddine, P. Nath: Phys. Rev. Lett. **50**, 232 (1983); P. Fayet: Phys. Lett. **125B**, 178 (1983)
18. For a compilation, see: H. Küster: Thesis. Universität Karlsruhe (1987)
19. F.A. Behrends, R. Kleiss, S. Jadach: Nucl. Phys. **B202**, 63 (1982)
20. T. Sjöstrand: Comp. Phys.. Comm. **27**, 243 (1982), **28**, 229 (1983). We used the updated version JETSET 5.2
21. G. Farrar, P. Fayet: Phys. Lett. **89B**, 191 (1980)
22. M.K. Gaillard et al.: Phys. Lett. **116B**, 279 (1982)
23. P. Fayet: Phys. Lett. **117B**, 460 (1982)
24. M. Glück, E. Reya: Phys. Lett. **130B**, 423 (1983)
25. J.A. Grifols, R. Pascual: Phys. Lett. **135B**, 319 (1984)
26. C. Weizsäcker: Z. Phys. **88**, 612 (1934); E.J. Williams: Proc. Roy Soc. Lond. **A139**, 169 (1933), Phys. Rev. **45**, 729 (1934); L. Landau, E. Lifshitz: Phys. Z. Soviet Union **6**, 244 (1934); P. Kessler: Nuovo Cimento **17**, 809 (1960)
27. Particle Data Group: Phys. Lett. **170B**, 1 (1986)
28. CELLO Coll., H.J. Behrend et al.: Phys. Lett. **183B**, 400 (1987)
29. C. Cremmer, P. Fayet, L. Girardello: Phys. Lett. **122B**, 41 (1983)
30. I.I. Bigi, S. Rudaz: Phys. Lett. **153B**, 335 (1984)
31. V. Barger et al.: Phys. Lett. **131B**, 372 (1983)
32. G. Eilam, E. Reya: Phys. Lett. **145B**, 425 (1984), (Erratum: **148B**, 502 (1984)). See also [25]
33. M. Martinez et al.: Z. Phys. C – Particles and Fields **29**, 309 (1985)
34. CELLO Coll., H.J. Behrend et al.: Phys. Lett. **161B**, 182 (1985)
35. E. Reya: Phys. Lett. **133B**, 245 (1983)
36. D.A. Dicus et al.: Phys. Rev. **D30**, 1112 (1984)
37. CELLO Coll., H.J. Behrend et al.: Preprint DESY 87-005, to be published
38. N. Cabibbo, G.R. Farrar, L. Maiani: Phys. Lett. **105B**, 155 (1981)
39. H. Komatsu, J. Kubo: Phys. Lett. **157B**, 90 (1985); H.E. Haber, G.L. Kane, M. Quiros: Phys. Lett. **160B**, 297 (1985)
40. E. Ros: Thesis. Universidad Complutense Madrid (1985). See also [14]
41. J. Ellis, J.S. Hagelin: Phys. Lett. **122B**, 303 (1983)
42. P. Fayet: Phys.. Lett. **175B**, 471 (1986)
43. J.S. Hagelin, G.L. Kane, S. Raby: Nucl. Phys. **B241**, 638 (1984); L.E. Ibanez: Phys. Lett. **137B**, 160 (1984)
44. M. Quiros, G.L. Kane, H.E. Haber: Nucl. Phys.. **B273**, 333 (1986)
45. CELLO Coll., H.J. Behrend et al.: Phys. Lett. **123B**, 127 (1983), CELLO Coll., H.J. Behrend et al.: Phys. Lett. **114B**, 287 (1982)
46. JADE Coll., W. Bartel et al.: Z. Phys. C – Particles and Fields **29**, 505 (1985), JADE Coll., W. Bartel et al.: Phys. Lett. **152B**, 392 (1985) JADE Coll., W. Bartel et al.: Phys. Lett. **152B**, 385 (1985), JADE Coll., W. Bartel et al.: Phys. Lett. **146B**, 126 (1984), JADE Coll., W. Bartel et al.: Phys. Lett. **139B**, 327 (1984), MARK J Coll., B. Adeva et al.: Phys. Lett. **152B**, 439 (1984), MARK J. Coll., B. Adeva et al.: Phys. Rev. Lett. **53**, 1806 (1984), TASSO Coll., M. Althoff et al.: Z. Phys. C – Particles and Fields **26**, 337 (1984), TASSO Coll., R. Brandelik et al.: Phys. Lett. **117B**, 365 (1982)
47. For recent updates, see: W. de Boer: Proc. of the 17th Int. Symp. on Multiparticle Dynamics, Seewinkel, Austria (1986), and preprint MPI-PAE/Exp. El. 167; M. Davier: Proc. of the 23rd Int. Conf. on High Energy Physics, Berkeley (1986), and preprint LAL 86-31; J.F. Grivaz: ibid. and preprint LAL 86-28; S. Whitaker: ibid. and preprint BUHEP 86-10
48. ASP Coll., G. Bartha et al.: Phys. Rev. Lett. **56**, 685 (1986); MAC Coll., E. Fernandez et al.: Phys. Rev. Lett. **54**, 1118 (1985); MAC Coll., E. Fernandez et al.: Phys. Rev. Lett. **52**, 22 (1984); MARK II Coll., L. Gladney et al.: Phys. Rev. Lett. **51**, 225 (1983)
49. A. Honma: Proc. of the 23rd Int. Conf. on High Energy Physics, Berkeley (1986), and preprint CERN EP/86-153